Meteorologische Zeitschrift, Vol. **10**, No. 3, 187-192 (June 2001)

Article

Boundary layer photochemistry during a total solar eclipse

PETER FABIAN[1,*], BERNHARD RAPPENGLÜCK[1], ANDREAS STOHL[1], HERBERT WERNER[1], MARTIN WINTERHALTER[1], HANS SCHLAGER[2], PAUL STOCK[2], HARALD BERRESHEIM[3], UWE KAMINSKI[3], PETER KOEPKE [4], JOACHIM REUDER[4] and WOLFRAM BIRMILI[5]

[1] Technische Universität München, Bioklimatologie und Immissionsforschung, Germany
[2] Institut für Physik der Atmosphäre, DLR, Oberpfaffenhofen, Germany
[3] Meteorologisches Observatorium Hohenpeißenberg, Germany
[4] Universität München, Germany
[5] Institut für Troposphärenforschung, Leipzig, Germany

(Manuscript received May 31, 2000; in revised form November 28, 2000; accepted December 3, 2000)

Abstract

Simultaneous measurements of radiation, photolysis frequencies, O_3, CO, OH, PAN and NO_x species were carried out in the boundary layer, along with pertinent meteorological parameters, under total solar eclipse conditions. This experiment performed at about 34°solar zenith angle and noontime conditions thus provided a case study about the interactions between radiation and photochemistry under fast "day-night" and "night-day" transitions, at high solar elevation. The results reveal a close correlation of photolysis frequencies $j_{O(^1D)}$and $j_{NO_2}$with the UV radiation flux. All three parameters show, due to the decreasing fraction of direct radiation at shorter wavelengths, much weaker cloud shading effects than global solar radiation. NO and OH concentrations decrease to essentially zero during totality. Subsequently, NO and OH concentrations increased almost symmetrically to their decrease preceding totality. The NO/NO_2 ratio was proportional to j_{NO_2}over ±30 min before and after totality indicating that the partitioning of NO_x species is determined by j_{NO_2}. Simple box model simulations show the effect of reduced solar radiation on the photochemical production of O_3 and PAN.

Zusammenfassung

Während der totalen Sonnenfinsternis am 11. August 1999 wurden simultane und kontinuierliche Messungen von O_3, CO, OH, PAN and NO_x, Strahlung, Photolysefrequenzen und relevanten meteorologischen Parametern durchgeführt. Dieses Experiment, durchgeführt etwa am Mittag, bei 34°Zenithwinkel der Sonne, ermöglichte die Untersuchung der Interaktion von Strahlung und Photochemie für schnelle Tag-Nacht und Nacht-Tag-Übergänge bei hohem Sonnenstand. Die Ergebnisse zeigen eine enge Korrelation der Photolysefrequenzen $j_{O(^1D)}$und j_{NO_2}mit dem UV-Strahlungsfluss. Alle drei Parameter zeigen, wegen des abnehmenden Anteils direkter Sonnenstrahlung bei kurzen Wellenlängen, erheblich geringere Abschwächung durch Wolken als die Globalstrahlung. NO und OH gehen während der Verdunkelungsphase auf Null herunter. Danach steigen NO und OH nahezu symmetrisch zum vorherigen Abfall wieder an. Das NO/NO_2-Verhältnis war 30 min vor bis 30 min nach der Totalität proportional zu j_{NO_2}und zeigte damit, dass die Partitionierung von NO_x durch j_{NO_2}bestimmt wurde. Mit einem einfachen Boxmodell wurde der Effekt der reduzierten Sonnenstrahlung auf die photochemische Produktion von O_3 und PAN berechnet.

1 Introduction

On August 11, 1999, a total solar eclipse happened in parts of Europe and Asia. At Freising-Weihenstephan (WHS) (Lat. 48°24'5"N, Long. 11°43'10"E), 30 km NE of Munich, it occurred at 10:37 UT (12:37 CEST), with totality lasting 2.3 minutes, at a solar zenith angle of 34°, enabling us to investigate photochemical processes under fast daylight-to-darkness and darkness-to-daylight transitions. Within BAYSOFI (**Bay**erische **So**nnen**fi**nsternis), an interdisciplinary field campaign focussed on the effects of the total eclipse (see FABIAN et al., this issue), measurements of radiation, photolysis rates, O_3, CO, PAN, NO_x and meteorological parameters were carried out at WHS. Simultaneously, measurements of OH along with other chemical and meteorological parameters were conducted at the Meteorological Observatory Hohenpeißenberg (MOHp) about 60 km SW of WHS. At MOHp the eclipse reached 99% of totality. For logistic reasons, the OH instrument could

* Corresponding author: Peter Fabian, Lehrstuhl für Bioklimatologie und Immissionsforschung, Technische Universität München, Am Hochanger 13, 85354 Freising-Weihenstephan, Germany, e-mail: fabian@met.forst.tu-muenchen.de

0941-2948/01/0010-0187 $ 02.70
DOI: 10.1127/0941-2948/2001/0010-0187

Table 1: Mixing ratios (ppb) of some important species used to initialize the photochemical box model.

Compound	*Mixing ratio*
NO_2	3.5
NO	1.0
PAN	0.1
O_3	30
HONO	0.4
HNO_3	0.2
CO	110
CH_4	1800
Ethane	1.40
Propane	1.00
n-Butane/i-Butane	0.14
Pentane	0.11
Toluene	0.30
Xylene	0.12
Isoprene	0.30

not be transferred to WHS. Thus for comparison of the MOHp and WHS data, certain restrictions apply.

2 Measurements and results

For both WHS and MOHp meteorological and air chemistry data from previous measurement campaigns are documented (FABIAN et al., 1998; RAPPENGLÜCK and FABIAN, 1999). WHS is close to the small town of Freising, whereas MOHp is located on top of the Hohenpeißenberg mountain (1000 m a.s.l.), about 300 m above the surrounding rural terrain. The instruments used are listed in Table 1 within FABIAN et al., 2001.

Fig. 1 shows pertinent information on the meteorological conditions before, during and after the total solar eclipse at the Weihenstephan site. Both during morning and afternoon of August 11, cloudy conditions prevailed, with large fluctuations of the global radiation *G*. With the onset of the eclipse (first contact at 09:17 UT) the cloud cover diminished. Cloud sections obscured the sun between 09:45 and 09:55 UT, but from 10:00 onwards, towards totality and during the first phase of reappearing sun, cumulus clouds vanished leaving only some altostratus clouds allowing to observe the event. Clouds reappeared after 11:10 UT. During the final phase of the eclipse the wind velocity dropped from 5 m/s to 2 m/s, and temperatures decreased by about 3 K. This temperature drop was derived taking into account the diurnal temperature variation. It can be seen directly from the measurements shown in Fig. 5 of FABIAN et al., 2001.

The photolysis frequencies $j_{O(^1D)}$und $j_{NO_2}$and the UV radiation flux are closely correlated, showing the

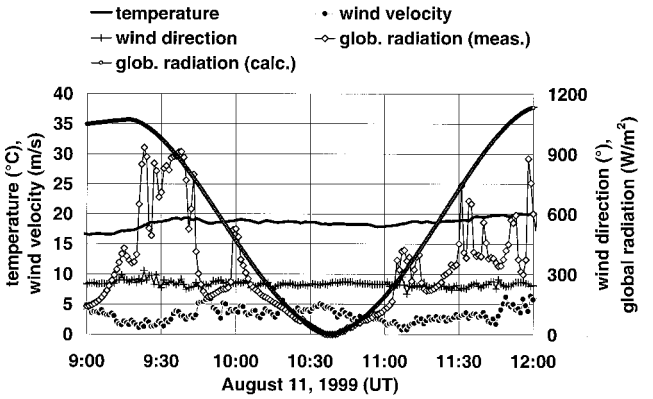

Figure 1: Meterological measurements obtained at WHS. This presentation also includes the global radiation as calculated for the WHS site based on astronomical data.

same temporal structure as *G* due to cloud effects (Fig. 2). The magnitude of the cloud effect decreases towards shorter wavelengths due to the decreasing portion of direct radiation and is lower for the actinic flux than for the irradiance (KOEPKE et al., 2001). Thus, while *G* was reduced by about 70% from its cloudless level, the corresponding reductions in UV radiation and $j_{O(^1D)}$were about 50% and 30–40%, respectively. During totality all observed radiation quantities were below the instrument detection limits. With *G* close to zero, the radiation budget (not shown) became negative, similar to nighttime conditions.

Fig. 3 shows the temporal behaviour of the chemical species of interest, along with the UV radiation changes. With about 100 ppb of CO and 5 ppb of NO_x, the pollution level was moderate. O_3 fluctuated between 30 and 40 ppb, showing a sudden increase by about 10 ppb during totality. Measured NO and NO_2 agreed such that their sum matched measured NO_x well. As NO became zero NO_x showed almost the same values, indicating that NO_x was composed of NO_2 only during totality. It should be noted that for measuring NO a high-sensitivity chemiluminescence instrument with a very low detection limit of only 3 pptv was used (Table 1 of FABIAN et al., 2001). With this instrument the zero signal due to interferences of chemiluminescence reactions with trace

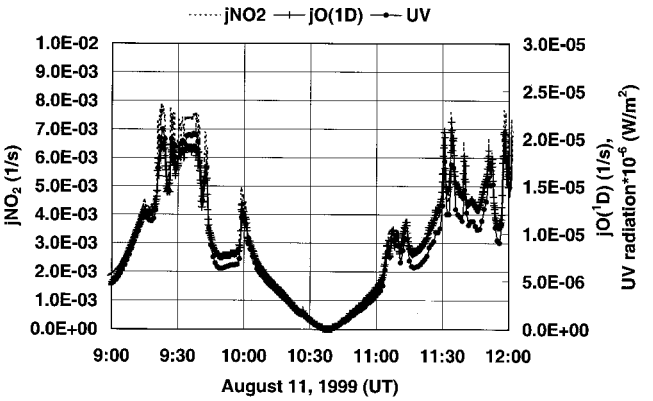

Figure 2: Measurements of j_{NO_2}, $j_{O(^1D)}$and UV-radiation at WHS.

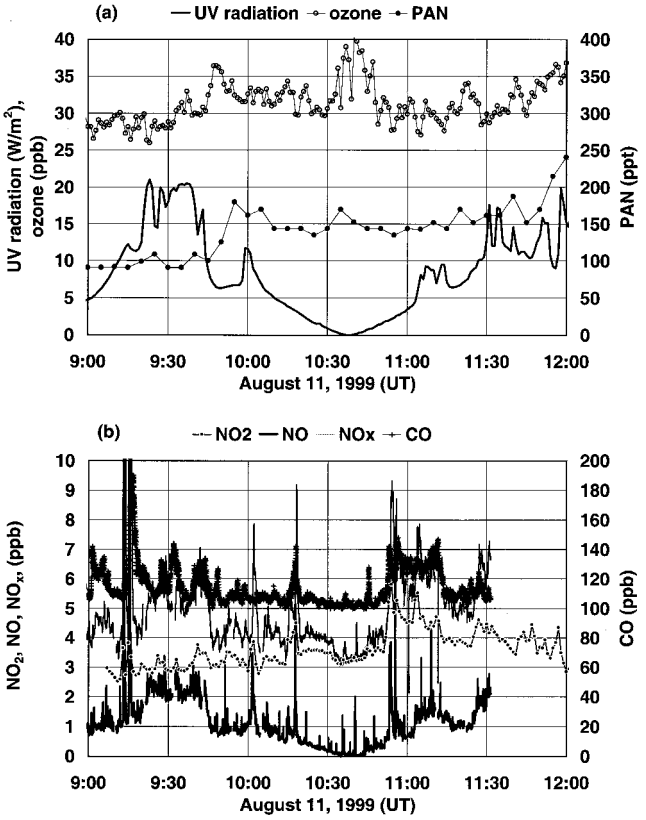

Figure 3: Air chemistry data obtained at WHS.

gases other than NO is largely reduced by using a zeroing chamber which can be inserted into the sample gas flow. Inside the zeroing volume NO is completely oxidized to NO_2, and cross-chemiluminescence reactions can be determined during this time in the main reaction chamber. Thereby, the partitioning between NO and NO_2 as a function of j_{NO_2}could be measured during BAYSOFI over the entire period of the solar eclipse.

The decrease of NO_x, from about 5 ppb before 09:45 to 3 ppb during the eclipse, accompanied by a similar decrease of CO, is due to almost complete cessation of local NO_x sources, mostly automobiles, because of drivers watching the eclipse. Two distinct spikes of NO_x and CO at 10:05 and 10:20 UT originate from taxicabs carrying visitors to the measuring site. When the sun started reappearing, at about 10:50 UT, people started driving, and NO_x and CO levels rose again. PAN shows moderate levels of about 140 ppt. The peak of 170 ppt during totality is difficult to reconcile with the other data. Similarly, the 10 ppb O_3 increase during totality cannot be explained based on the NO_x behaviour alone, as 3 to 4 ppb of NO_x is not sufficient to account for about 10 ppb of O_3 titration. Certainly, these peaks are no artefacts, since O_3 and PAN were measured independently with different instruments (see Table 1 of FABIAN et al., 2001). Thus it appears that the O_3 and PAN peaks observed during totality are due to advection. Based on our own measurements, vertical transport is unlikely, as the wind velocity is decreasing during the event, while the wind direction remains fairly constant. Furthermore, the simultaneous PAN increase, by about 30 percent similar to that of O_3, makes downward mixing very unlikely. Downward mixing can nearly be excluded from the measurements by WINKLER et al. (2001) and FOKEN et al. (2001) who found, during the solar eclipse, decreasing winds up to 50 m in altitude and a tendency towards stabilization and decreasing vertical extent of the mixing layer. Thus horizontal advection remains as the most likely cause.

Meteorological and chemical parameters were also measured at the MOHp site (WINKLER et al., 2001). Fig. 4 shows OH concentrations and $j_{O(^1D)}$at MOHp. With the exception of a few short-term interruptions in the OH measurements due to intermittent rain showers, decreasing OH levels could well be resolved during the eclipse. Overall, following the statistical interpretation by EHHALT and ROHRER (2000), 74% of the OH variation could be explained by variations in solar UV with O3 photolysis most likely being the predominant source of OH. NO_x levels were mostly low (around 1 ppb) but increased to 2–4 ppb between 12:30–13:30 UT (not shown). At the same time, OH levels decreased significantly because of both lower $j_{O(^1D)}$and enhanced removal of OH by reaction with NO_2. With partially cloudy conditions at MOHp maximum $j_{O(^1D)}$levels ($1.45 \cdot 10^{-5}$ s^{-1}, measured at 12:33 UT) were lower than at WHS.

Gaseous H_2SO_4, a major precursor for atmospheric sub-micrometer particles, was also measured with the CIMS instrument (BERRESHEIM et al., 2000) and showed a diurnal variation very similar to that of OH (Fig. 4), but no correlation with SO_2. Fig. 4 also shows both measured and calculated H_2SO_4 concentrations. The major source of gaseous sulphuric acid in the atmosphere is oxidation of SO_2 by OH, its major sink is diffusive deposition onto aerosol particles. With respect to the latter process the average atmospheric lifetime of H_2SO_4 (corresponding to 1/kaw, see equation below)

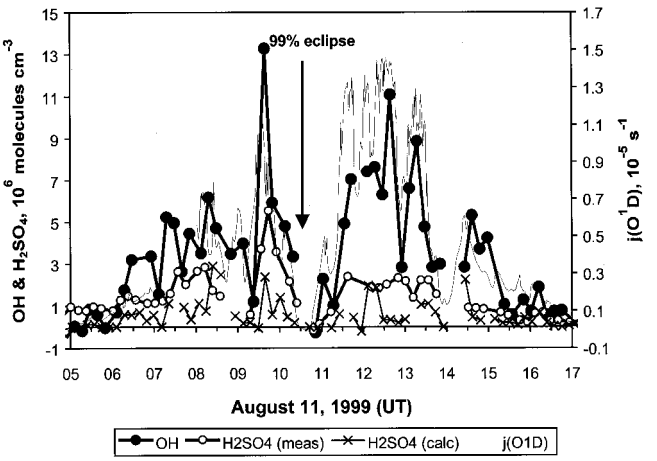

Figure 4: Diurnal variations of the OH and H_2SO_4 concentrations and the ozone photolysis frequency $j_{O(^1D)}$measured at Hohenpeißenberg (MOHp) on August 11, 1999.

was calculated to be 3–4 min. The sink rate was determined from the measured particle size distribution (3–800 nm) based on the DAHNEKE interpolation formula for vapour diffusion, and particle sizes being adjusted to ambient relative humidity. See BIRMILI et al. (2000) for more information on the aerosol measurements and balance calculations. The above time scale is typical for the lifetime of H_2SO_4 in the continental background atmosphere. With OH levels rapidly declining during the eclipse, H_2SO_4 concentrations also decreased rapidly. Assuming steady-state conditions between H_2SO_4 production and loss rates a simple balance equation was used to calculate H_2SO_4 levels based on measured SO_2, OH, and aerosol number concentrations:

$$\frac{k[SO_2][OH]}{kaw} = [H_2SO_4]$$

where the numerator on the left hand side represents the production term with $k = 8.5^{-13}$ cm^3 molec^{-1}s^{-1} (DEMORE et al., 1997) and kaw in the denominator represents the pseudo-first-order depositional rate constant. The results show values which were mostly somewhat lower than the measured H_2SO_4 levels. This difference could be due to errors in the measurements and/or an overestimate of the (dry) depositional loss of H_2SO_4 to aerosol particles.

Photochemical box model calculations were performed to simulate the variations of species of interest for WHS conditions. The model is a simplified zero-dimensional version of a Lagrangian 1-D model (STOHL et al., 1996; WOTAWA et al., 1998), employing an updated RADM scheme (STOCKWELL and KLEY, 1994). Two free-running (i.e. species concentrations were not nudged towards observed data after initialization) simulations were made. Both were initialized at 9:00 UT with mixing ratios either measured or assumed to be typical for the prevailing conditions at WHS as given in Table 1. No emissions or deposition were assumed to occur during the simulation period. The first run was driven by temperature, relative humidity, ambient pressure and j_{NO_2} (photolysis frequencies of other species were scaled to j_{NO_2} using solar zenith angles) as measured at WHS. For the second simulation measured photolysis frequencies were modified in order to represent identical atmospheric conditions but without reduction of the solar flux due to the eclipse, preserving variations in photolysis frequencies caused by variability in cloud cover. Photolysis frequencies for no eclipse conditions (ne) were determined using the measurements (e) according to:

$$j_{NO_2-ne} = \frac{j_{NO_2-e}}{R_{390nm}} \quad \text{(R1)}$$

$$j_{O(^1D)-ne} = \frac{j_{O(^1D)-e}}{R_{310nm}} \quad \text{(R2)}$$

R, the ratio between the extraterrestrial radiation with the sun covered by the moon and the extraterrestrial radiation without coverage, is calculated taking into account the effect of spectrally dependent limb darkening

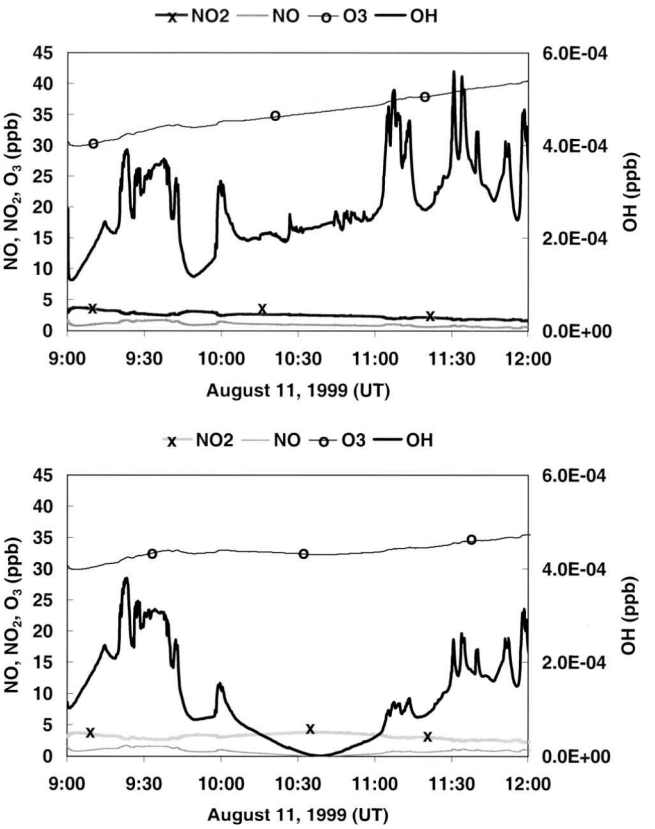

Figure 5: Model results: upper panel without the effects of the total solar eclipse, lower panel including the effects of the total solar eclipse.

(KOEPKE et al., 2001). During about 15 minutes centered around totality, the uncertainty in photolysis frequencies, modified following equations R1 and R2, is high. Therefore data points exceeding a 30% error derived by Gaussian error propagation, were replaced by constant values of $1.52 \cdot 10^{-5}$ s^{-1} for $j_{O(^1D)}$ and $5.2 \cdot 10^{-5}$ s^{-1} for j_{NO_2}, representing average conditions of the time intervals before and after totality (KOEPKE et al., 2001). For this second simulation, temperatures were assumed to be higher than the observed ones. A maximum temperature increase of 3.5 K was assumed to occur 45 minutes after totality, and no increase was applied 30 minutes before and two hours after totality. However, the model results were only moderately sensitive to these temperature modifications.

Both simulations were run for six hours. Despite simplifications and the fact that this episode was dominated by strong advection, our results show the principle effects on tropospheric photochemistry caused by the eclipse (Fig. 5). With the eclipse, a net O_3 production of 6 ppb until 12:00 UT and 11 ppb until 15:00 UT is estimated, while with the eclipse being eliminated, the production was 10 ppb and 16 ppb, respectively. Most of the difference in O_3 production occurred during the eclipse at high solar zenith angles. However, even after the eclipse, O_3 production rates were somewhat higher in the second case due to the more active noon-time

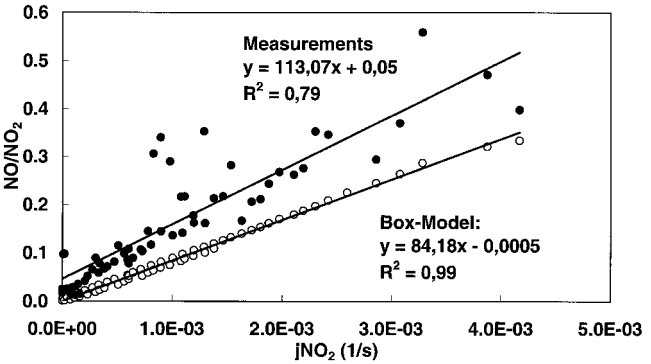

Figure 6: The NO/NO_2 ratio as a function of j_{NO_2} during 10:15–10:45 UT. Measurements displayed as thick line/full circles and model results displayed as dashed line/open circles.

chemistry. Net PAN production was also higher without the eclipse (0.85 ppb) than with the eclipse (0.71 ppb).

Differences for PAN were smaller than for O_3, partly because thermal decomposition of PAN was enhanced due to the higher temperatures. This effect, however, was found to be very small: additional model runs under eclipse conditions but 3.5 K higher temperatures showed PAN reductions of less then 1.5% only. Thus at any rate it can be concluded that the afore mentioned PAN peak observed during totality cannot be due to reduced thermal decay as a result of the slight temperature drop, leaving advection the only likely cause.

Changes of NO and NO_2 were investigated considering the basic photochemical equilibrium reactions

$$NO + O_3 \rightarrow NO_2 + O_2 \quad k_3 \qquad \text{(R3)}$$

$$NO_2 + h\nu \rightarrow NO + O \quad j_{NO_2} \qquad \text{(R4)}$$

$$O + O_2 + M \rightarrow O_3 + M \quad k_5 \qquad \text{(R5)}$$

which control the partitioning of NO and NO_2:

$$\frac{NO}{NO_2} = \frac{j_{NO_2}}{k_3 O_3} \qquad \text{(R6)}$$

NO/NO_2 is controlled by j_{NO_2}, as k_3 depends only on temperature which varied little during the eclipse, O_3 fluctuated by 30% in the measurements and less in the model runs, while j_{NO_2} varied by more than an order of magnitude. Minor deviations from R6 are caused by peroxy radical reactions. Fig. 6 shows NO/NO_2 for both the measurements and the model results plotted as a function of j_{NO_2}. The strong linear correlation confirms that the NO_x partitioning is indeed controlled by j_{NO_2}. The larger scatter in the measurement data is due to the stronger O_3 fluctuations and the combined uncertainties of all measurements. However, the modeled slope is smaller by 30% than the measured one which cannot be explained by differences in O_3 or measurement uncertainties alone. Rather it suggests an overestimate of the rate constant k_3.

3 Concluding remarks

The reduced solar radiation during the eclipse significantly affected the photochemical production of PAN and O_3. Photochemical box model simulations suggest a 4 ppb reduction in net O_3 production until the end of the eclipse and 5 ppb until the afternoon. Both measurements and model simulations show that the partitioning of NO_x between NO and NO_2 was determined almost exclusively by the variations in j_{NO_2}. Besides illustrating a case study on the interaction between radiation and photochemistry under fast day-night and night-day transitions at high noontime solar elevations, our experiment shows interesting aspects of temporarily almost vanishing and later reappearing local emissions, at quite moderate overall pollution levels, in agreement with our overall understanding of atmospheric processes. The O_3 and PAN peaks observed almost simultaneously during totality can only partly be explained by photochemistry, because neither NO_x titration of O_3 nor change of thermal decay of PAN can account for the 30 percent increase of both species. As downward mixing can be ruled out, horizontal advection remains as the most likely cause of this interesting effect.

Acknowledgments

OH data from MOHp were provided by T. ELSTE, NO_x data by S. GILGE.

References

BERRESHEIM H., T. ELSTE, C. PLASS-DÜLMER, F.L. EISELE, D.J. TANNER, 2000: Chemical ionization mass spectrometer for long-term measurements of atmospheric OH and H_2SO_4. – Int. J. Mass Spec. **202**, 91–109.

BIRMILI, W., A. WIEDENSOHLER, C. PLASS-DÜLMER, H. BERRESHEIM, 2000: Evolution of newly formed particles in the continental boundary layer: A case study including OH and H_2SO_4 measurements. – Geophys. Rev. Lett. **27**, 2205–2208.

DEMORE, W.B., S.P. SANDER, D.M. GOLDEN, R.F. HAMPSON, M.J. KURYLO, C.J. HOWARD, A.R. RAVISHANKARA, C.E. KOLB, M.J. MOLINA, 1997: Chemical kinetics and photochemical data for use in stratospheric modeling. – JPL Publ. **97-4**, Jet Propulsion Laboratory, Pasadena, USA.

EHHALT, D.H., F. ROHRER, 2000: Dependence of the OH concentration on solar UV. – J. Geophys. Res. **105**, 3565–3571.

FABIAN P., B. RAPPENGLÜCK, P. SUPPAN, G. JAKOBI, M.M. HIRSCHBERG, H. REITMAYER, J. REUDER, L. KINS, G. BRUNNENMANN, R. DLUGI, M. WIEGNER, V. FREUDENTHALER, J. ACKERMANN, D. RABUS, W. VÖLKER, L. LEHMANN, W. VÖGLER, T. AMLONG, A. HUBER, R. KOTZICK, B. FRÖSCHL, C. KOPP, R. NIESSNER, M. WELLER, J. LATTAUSCHKE, H. RENTSCH, W. JUNKERMANN, 1998: Ozonbildung und Partikel im Photosmog (OPAP). – Bay. Staatsmin. f. Landesentwicklung u. Umweltfragen, Final Report, 79 pp.

FABIAN, P., M. WINTERHALTER, B. RAPPENGLÜCK, H. REITMAYER, A. STOHL, H. SCHLAGER, P. KOEPKE, TH. FOKEN, B. WICHURA, H. BERRESHEIM, K.-H. HÄBERLE, R. MATYSSEK, TH. KARTSCHALL, 2001: The BAYSOFI Campaign – Measurements carried out during the total solar eclipse of August 11, 1999. – Meteorol. Z. **10**, 165–170.

FOKEN, TH., B. WICHURA, O. KLEMM, J. GERCHAU, M. WINTERHALTER, T. WEIDINGER, 2001: Micrometeorological measurements during the total solar eclipse of August 11, 1999. – Meteorol. Z. **10**, 171–178.

KOEPKE, P., J. REUDER, J. SCHWEEN, 2001: Spectral variation of the solar radiation during an eclipse. – Meteorol. Z. **10**, 179–186.

RAPPENGLÜCK B., P. FABIAN, 1999: Non Methane Hydrocarbons (NMHC) in the Greater Munich Area/Germany. – Atmos. Environ. **33**, 3843–3857.

STOCKWELL, W.R., D. KLEY, 1994: The Euro-RADM mechanism. A gas-phase chemical mechanism for European air quality studies. – Berichte des Forschungszentrums Jülich **2686**, Research Centre Juelich, Germany, 114 pp.

STOHL, A., E. WILLIAMS, G. WOTAWA, H. KROMP-KOLB, 1996: A European inventory of soil nitric oxide emissions and the effect of these emissions on the photochemical formation of ozone in Europe. – Atmos. Environ. **30**, 3741–3755.

WINKLER, P., U. KAMINSKI, U. KÖHLER, J. RIEDL, H. SCHROERS, D. ANWENDER, 2001: Development of meteorological parameters and total ozone during total eclipse of August 11, 1999. – Meteorol. Z. **10**, 193–199.

WOTAWA, G., A. STOHL, B. NEININGER, 1998: The urban plume of Vienna: comparison between aircraft measurements and photochemical model results. – Atmos. Environ. **32**, 2479–2489.